NANO LETTERS
Letter
Cite This: Nano Lett. XXXX, XXX, XXX−XXX
pubs.acs.org/NanoLett

Picosecond Charge Transfer and Long Carrier Diffusion Lengths in Colloidal Quantum Dot Solids

Andrew H. Proppe,[†,‡] Jixian Xu,[‡] Randy P. Sabatini,[‡] James Z. Fan,[‡] Bin Sun,[‡] Sjoerd Hoogland,[‡] Shana O. Kelley,[†,§] Oleksandr Voznyy,*[,‡] and Edward H. Sargent*[,‡]

[†]Department of Chemistry, University of Toronto, 80 St. George Street, Toronto, Ontario Canada, M5S 3G4

[‡]The Edward S. Rogers Department of Electrical and Computer Engineering, University of Toronto, 10 King's College Road, Toronto, Ontario Canada, M5S 3G4

[§]Department of Pharmaceutical Sciences, Leslie Dan Faculty of Pharmacy, University of Toronto, Toronto, Ontario Canada, M5S 3M2

Supporting Information

ABSTRACT: Quantum dots (QDs) are promising candidates for solution-processed thin-film optoelectronic devices. Both the diffusion length and the mobility of photoexcited charge carriers in QD solids are critical determinants of solar cell performance; yet various techniques offer diverse values of these key parameters even in notionally similar films. Here we report diffusion lengths and interdot charge transfer rates using a 3D donor/acceptor technique that directly monitors the rate at which photoexcitations reach small-bandgap dot inclusions having a known spacing within a larger-bandgap QD matrix. Instead of relying on photoluminescence (which can be weak in strongly coupled QD solids), we use ultrafast transient absorption spectroscopy, a method where sensitivity is undiminished by exciton dissociation. We measure record diffusion lengths of ∼300 nm in metal halide exchanged PbS QD solids that have led to power conversion efficiencies of 12%, and determine 8 ps interdot hopping of carriers following photoexcitation, among the fastest rates reported for PbS QD solids. We also find that QD solids composed of smaller QDs (d = ∼3.2 nm) exhibit 5 times faster interdot charge transfer rates and 10 times lower trap state densities compared to larger (d = ∼5.5 nm) QDs.

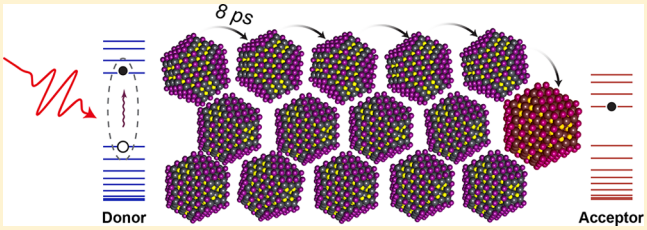

KEYWORDS: *Ultrafast spectroscopy, diffusion lengths, quantum dot photovoltaics, carrier transport, charge transfer*

Quantum dots (QDs) are a subject of longstanding interest for both fundamental physical chemistry and also next-generation optoelectronic devices. Bandgap tunability, colloidal stability, and surface functionalization allow them to be used in solution processed optoelectronic devices such as photovoltaics,[1−6] light-emitting diodes,[7−9] and photodetectors.[2,10] In solution, QDs are synthesized using long alkyl chain molecules, typically oleic acid, for colloidal stability.[11] In films, this results in large interdot distances and insulating barriers that impede exciton dissociation and carrier transport.[12,13] Solution-phase ligand exchange protocols have been developed whereby oleic acid on the QD surface is replaced by halide ligands in a biphasic solution, facilitating the preparation of concentrated QD inks.[14] This has resulted in QD photovoltaics with high power conversion efficiencies recently certified at 12.0%.[15]

Solution-phase exchanges enable the formation of thick active layers (>300 nm) and ensure fuller surface coverage of QDs with halides. This enables greater densification of the QD solid resulting in stronger interdot coupling,[16] which leads to faster exciton dissociation and carrier transfer rates. One of the most important metrics in a photovoltaic device is the diffusion length, L_D, of the carriers, which should exceed the thickness of the active layer for highly efficient charge collection.[17] The diffusion length is related to the mobility of the carriers and their lifetime by the following formula

$$L_D = \sqrt{D\tau} \quad (1)$$

where D is the diffusion coefficient and τ is the lifetime of the carrier. D is related to carrier mobility via the Einstein relation

$$D = \frac{kT\mu}{q} \quad (2)$$

where k is the Boltzmann constant, T is temperature, μ is carrier mobility, and q is the charge of the carrier. There are numerous reported measurements of mobilities and charge carrier lifetimes in QD solids.[18−22] These often rely on techniques that probe the QD solid at a device level, for example, in a field-effect transistor (FET) architecture or using Hall effect measurements. These methods rely on carrier

Received: July 24, 2018
Revised: October 20, 2018
Published: October 25, 2018

DOI: 10.1021/acs.nanolett.8b03020
Nano Lett. XXXX, XXX, XXX−XXX

injection to fill shallow traps and thus do not fully account for the effect of polydispersity on transport, which can greatly influence carrier mobilities when transport predominantly occurs by interdot carrier hopping between localized states.[18,23] Further, the active layer is typically probed at operating conditions different from those of a QD solar cell, and interfacial defects and traps between the active layer and contacting electrodes may also affect measured mobilities and lifetimes.[17]

Optical methods offer an attractive alternative to electrical methods, because interfacial defects are obviated, and low photoexcitation fluences can more closely mimic solar illumination conditions. Such methods have proven to be successful for determining diffusion lengths in QD solids.[24−26] Introducing fixed amounts of smaller bandgap acceptor QDs into the QD active layer and monitoring how the donor/acceptor photoluminescence (PL) ratio changes with increasing acceptor concentration allows for the determination of carrier mobilities and lifetimes.[25] However, utilizing PL ratios still has limitations: QD solids with excellent transport properties, despite low trap state densities, can have very low photoluminescence quantum yield (PLQY) owing to rapid exciton dissociation, which can occur within a few hundred picoseconds for strongly coupled QDs,[27−29] followed by migration of free carriers to traps where they recombine nonradiatively, eliminating most of the PL signal.[30] This can make determining the ratio of donor:acceptor PL intensity unreliable. In time-resolved PL measurements using time-correlated single photon counting (TCSPC), rapid (sub-ns) lifetimes can eliminate almost the entirety of the PL signal,[31] preventing an optical measurement of τ which should be in the range of 10 to 100s of ns.[27,31,32]

Here, to overcome these limitations but maintain the usage of a contactless and purely optical technique to determine carrier diffusion lengths, we use a combination of ultrafast and microsecond transient absorption spectroscopy (TAS). The bandedge bleach signal in TAS, whose amplitude is representative of the bandedge carrier population,[28] persists for both excitons and unbound electron−hole pairs,[33] and is thus is sensitive to the presence of electrons and holes but does not depend on their recombination for detection. The signal amplitude is therefore not strictly dependent on PLQY, allowing measurements on low-PLQY QD solids at device level thicknesses with low excitation fluences. The change in donor QD lifetime with varying concentrations of acceptor QDs provides the diffusion coefficient and mobility. Population transfer can be monitored directly by following the decay (rise) in the spectrally distinct donor (acceptor) QD bleach signals, and interdot transfer rates can be determined by modeling the number of hops that occur in the time it takes for carriers to transfer to the acceptor QDs. We use this technique to measure diffusion coefficients and carrier lifetimes for QD solids composed of two different sizes of PbS QDs, and find record diffusion lengths of 300 ± 30 nm for 1.3 eV bandgap (3.2 nm dot size) PbS QD solids used in solar cells with certified power conversion efficiencies of 12.0%.[15] We also measure ∼8 ps interdot hopping times and sub-10 ps spectral diffusion following photoexcitation, which are among the fastest charge transfer rates in PbS QD solids. For larger 0.95 eV bandgap (5.5 nm dot size) PbS QDs, which are emerging as promising candidate materials to harvest infrared photons with energies below the bandgap of crystalline silicon,[34−36] we find longer interdot hopping times of ∼50 ps and therefore lower mobilities compared to smaller QDs. Additionally, we find a 10 times greater trap state density in these larger QD materials that results in shorter lifetimes and lower diffusion lengths of ∼90 nm. This indicates that IR bandgap QDs do not only suffer from lower mobilities, but current ligand exchange methods that lead to record efficiency NIR QD solar cells[1,15] are not as effective at maintaining lower trap state densities in QD solids composed of larger dots.

Details of the QD synthesis, ligand exchange, preparation of the donor:acceptor mixtures, and spin coating of the thin films used in this study can be found in the Methods section. Briefly, the QDs undergo a biphasic solution-phase ligand exchange with PbI_2 to passivate the surface with atomic halide ligands before being redispersed as a concentrated solution and spin coated into thin films.[37] Absorbance and photoluminescence spectra of the QDs in solution before and after exchange, as well as in thin films, can be found in the Supporting Information (Figure S1). All films used in this study followed identical fabrication procedures for the QD active layers used in high efficiency photovoltaic devices, resulting in thicknesses of 350−400 nm (Figure S2).[1,34]

We expand upon the 3D model of Zhitomirsky et al.[24,25] used to extract carrier mobilities from PL ratios of donor/acceptor QD blends. The capture rate of carriers into traps (interchangeable with acceptor QDs) is the inverse of the trapping lifetime τ_{trap}^{-1} and in the Shockley−Read−Hall recombination model can be expressed as

$$k_{trap} = \tau_{trap}^{-1} = V_{th}\sigma N_t \tag{3}$$

where V_{th} is the thermal velocity in the hopping regime, also expressed as $V_{th} = d/\tau_{hop}$ with interdot distance d and the interdot hopping time τ_{hop}. N_t is the density of traps. σ is the capture cross section, which for the 3D model is assumed to be $1/4\pi d^2$.[25] Mobility μ is expressed as[38]

$$\mu = \frac{qd^2}{6\tau_{hop}kT} \tag{4}$$

From the Einstein equation relating D and μ

$$V_{th} = \frac{6D}{d} \tag{5}$$

D can then be obtained as

$$D = \frac{dV_{th}}{6} = \frac{d}{6\sigma\tau_{trap}N_t} \tag{6}$$

To extract D experimentally, we vary the density of traps N_t by introducing the quenching acceptor QDs and measuring the change in lifetime by following the bandedge bleach signal of the donor QDs. While it is possible to obtain D from a single measurement on a film with a given N_t, we perform measurements on at least four films with different N_t (varying over an order of magnitude) in order to calculate a more consistent value for D. We assume that these acceptor dots are homogeneously dispersed throughout a donor matrix since both donor and acceptor dots undergo the same ligand exchange in solution prior to being cast into a film, and the dot diameters are generally within ∼2 nm of each other. TAS measurements performed with pulses impinging on both the front and back (substrate-side) of a 5% acceptor film (photoexciting at 400 nm) gave identical bleach peaks for donor and acceptor QDs (Figure S3), which is consistent with

DOI: 10.1021/acs.nanolett.8b03020
Nano Lett. XXXX, XXX, XXX−XXX

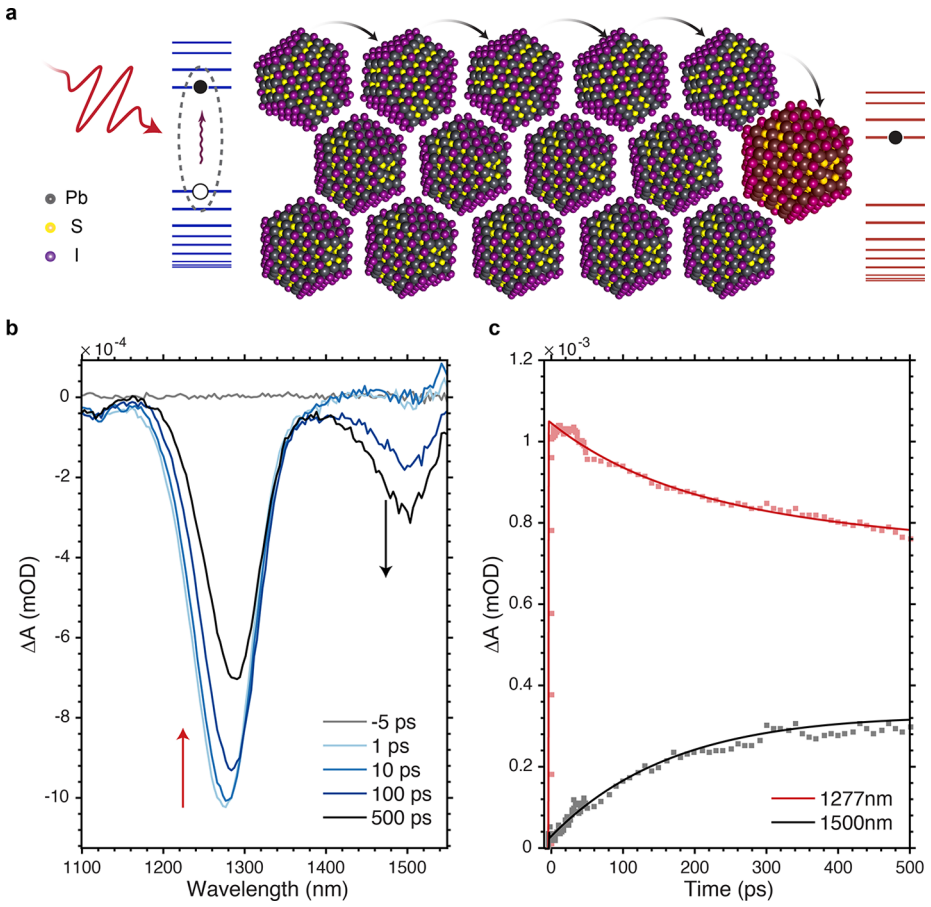

Figure 1. Probing carrier transfer in a donor/acceptor blend. (a) Photoexcitation at the exciton resonance of the donor QD generates excitons that rapidly dissociate into free carriers, which diffuse throughout the film. Electrons are eventually trapped in the acceptor QDs. (b) Transient absorption spectra at various delay times for a donor/acceptor blend of IR bandgap QDs, whereby the decay of donor signal and rise of the acceptor signal are simultaneously observed in this spectral window. (c) Time traces at the bleach signals for the donor QD (1277 nm) and the acceptor QD (1500 nm). The decay rate at the donor peak and the rise-time at the acceptor peak will not be identical because the acceptor rise-time will be convoluted with fast, higher order Auger recombination processes as the QDs become overloaded with carriers from the surrounding donor matrix.[44] For clarity, the raw data in these traces were smoothed with a moving average filter. Fits were obtained using unsmoothed data. Tracking the rise-time in 3.2 nm higher mobility QD solids for a donor:acceptor ratio of 99:1 similarly demonstrates negligible initial population of the acceptors from the photoexcitation pulse (Figure S5).

the acceptor QDs being isotropically dispersed throughout the donor matrix rather than a graded distribution (i.e., most of the acceptor QDs at the bottom of the film).[39,40]

The effective lifetimes observed in ultrafast TA measurements are assumed to be equal to the trapping lifetime in a film

$$\tau_{\text{eff}}^{-1} = \tau_{\text{radiative}}^{-1} + \tau_{\text{trap}}^{-1} \approx \tau_{\text{trap}}^{-1} \tag{7}$$

since τ_{trap} is usually tens or hundreds of ns in the acceptor-free film,[27,41] or hundreds of picoseconds when acceptors are introduced, which is much shorter than normal PbS QD PL lifetimes (>1 μs).[12] Since τ_{trap} and N_t are inversely related (assuming homogeneous dispersion of the acceptor QDs), in order to obtain a linear slope experimentally, we solve for D as

$$D = \frac{d}{6\sigma\tau_{\text{trap}}N_t} = \frac{d}{6\sigma\left(\tau_{\text{trap}}/N_t^{-1}\right)} \tag{8}$$

To extract carrier mobility from plots of τ_{trap} versus $1/N_t$, we introduce fixed concentrations of acceptor QDs into films that are otherwise comprised of donor QDs. Photoexcitation near the exciton resonance of the donor film will generate carriers that migrate throughout the film until they find an acceptor QD. In this work, we assume that photogenerated excitons dissociate before diffusing over multiple dots, owing to the small exciton binding energy in PbS[42] and the strong interdot coupling, and that all transport occurring is via charge transfer of free carriers. The donor:acceptor blend is illustrated schematically in Figure 1a. The injection of electrons from donor to acceptor is assumed to be rapid and irreversible owing to the large energy gap between donor and acceptor conduction bands (~300 meV, >10 kT). We note that in both our modified model here and the original one from which it is derived, we specifically focus on electron diffusion. Photoelectron spectroscopy measurements by Miller et al. on PbS QD films[43] show that the valence band energy is nearly equal in films made of QDs with bandgaps ranging between 1.0 and 2.5 eV, whereas the shifting in conduction band energies accounts for most of the change in the optical bandgap. Holes will then not be (irreversibly) trapped in acceptor dots owing to similar valence band energies.[24,43] This is consistent with our monoexponential rather than biexponential fits for trapping lifetimes, and our observation that photoexciting directly into smaller bandgap dots can still cause time-dependent bleaching in larger bandgap dots. We discuss both of these points in more detail below.

DOI: 10.1021/acs.nanolett.8b03020
Nano Lett. XXXX, XXX, XXX−XXX

Acceptors need to be introduced at sufficiently high concentrations such that the changes in lifetime are well-resolved in the 7.5 ns time window of our ultrafast TA experiments. The concentration range needed then depends on the mobility of the donor QD film: for example, in larger 5.5 nm QDs, acceptor QD concentrations (by weight percentage) of 1, 5, 10 and 15% are used. For higher mobility 3.2 nm QDs, acceptor concentrations are 0, 0.5, 1, 2 and 5%. We observe a linear correlation between trapping lifetime and trap percentage, which is consistent with homogeneously dispersed acceptors throughout the film (if acceptor QDs were aggregating and thus lowering the effective trap percentage, we would measure longer trapping lifetimes than expected from a linear trend).[25] Atomic force microscopy measurements show that the film roughness is unaffected by the introduction of these larger acceptor dots (Figure S2).

With sufficiently high acceptor concentrations, we observe bleach signal from the acceptor QDs as they are populated by diffusing carriers. Figure 1b demonstrates this for a blend of 90:10 donor/acceptor QDs with exciton resonances at 1277 and 1500 nm, respectively. In all experiments, we chose photoexcitation wavelengths nearly resonant with the donor QD exciton peak (930 nm photoexcitation for 950 nm bandgap QDs and 1270 nm photoexcitation for 1300 nm bandgap QDs) in order maximize the amount of light absorbed by the donors and minimize direct excitation of the acceptors. At early times (1−10 ps), there is minimal population of acceptor QDs directly excited from the photoexcitation pulse despite the fact that they comprise 10% of the film, because the absorbance of the donor QDs is roughly 25 times higher than the acceptor QDs at the photoexcitation wavelength (Figure S4). These dynamics are temporally tracked in Figure 1c, where the rise-time of the acceptors generally mirrors the decay of the donors.

Figure 2 shows the absorption spectra and kinetic traces from TA experiments in 3.2 nm PbS QDs solids with acceptor concentrations of 0, 0.5, 1.0, 2.0 and 5.0%. All measurements were performed with an excitation density of $\langle N \rangle = 0.001$ in order to minimize Auger recombination (Figure S6) but still obtain sufficient signal-to-noise ratios. The decay times are fit well by biexponential functions, besides the acceptor-free film, which is estimated by a monoexponential function. The second lifetime becomes shorter with increasing acceptor concentration, and the first (longer) lifetime remains relatively constant. The first lifetime extends well beyond the time window of these experiments and is attributed to the traps inherent to the QD film, which are much lower in density than the purposely introduced acceptors.[25] We note that the fit for the acceptor-free donor film is unreliable owing to the limited time window. This lifetime corresponds to the τ_{trap} of the native film, which we will use in combination with the extracted D values to calculate L_D. We discuss later how we obtained carrier lifetimes using a modified TA setup. Because we expect only τ_{trap} to change upon mixing more acceptor QDs into the films and because all films were measured under identical conditions, we can subtract the dynamics of the acceptor-free QD film from the rest of the transient traces to isolate a single exponential corresponding to τ_{trap}. A single trapping lifetime supports our model treating only electron diffusion rather than both electrons and holes, as the mobility of these carriers usually differs in PbS QD solids.[28] The longer time dynamics are identical in all films as surmised from the fact that the curves after subtraction begin to become flat at later times, especially at higher acceptor concentrations (Figure 2c). The resulting trapping lifetimes lead to the expected linear curves when plotted against N_t^{-1}. Similar raw data and fits for the 5.5 nm QDs can be found in the Supporting Information (Figure S7, Table S3).

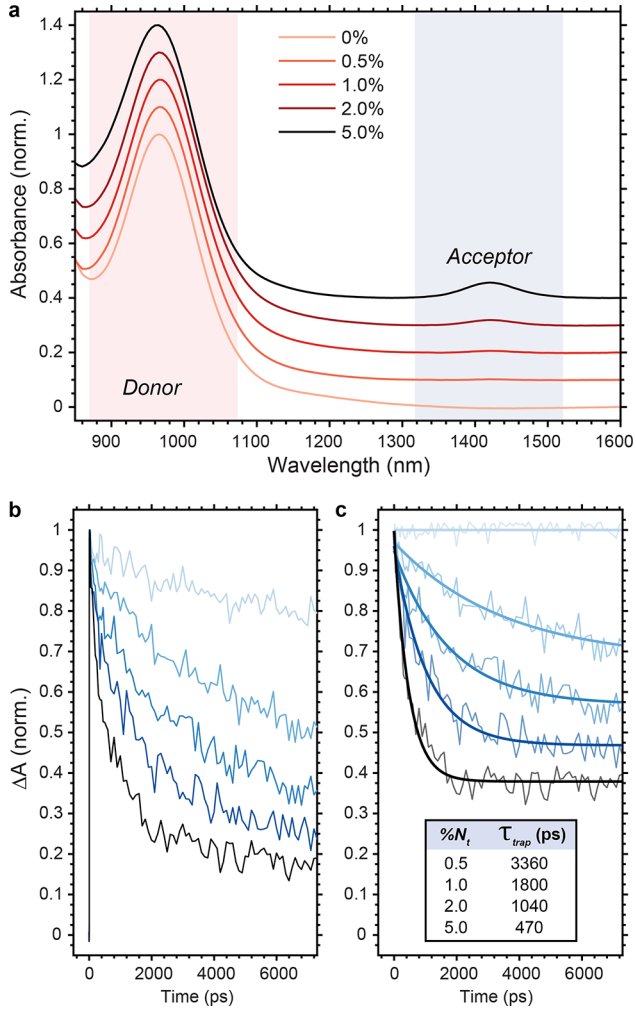

Figure 2. Mobilities from the dependence of carrier lifetime on trap percentage. Trap percentages represent the fraction of the solid that is comprised of larger (acceptor) QDs. (a) Absorption spectra of donor:acceptor films with 950 nm donors and ∼1400 nm acceptors. Spectra are normalized at the donor QD exciton peak and then offset for clarity. Donor/acceptor mixtures were prepared according to Table S1 in the Supporting Information. (b) Kinetic traces at the exciton bleach peak of 950 nm bandgap QD donor films with a range of acceptor QD concentrations, increasing from top (0%) to bottom (5%). (c) Data with fits after subtracting the acceptor-free dynamics from each trace. Fitting parameters can be found in Table S2.

Because the carrier lifetime of the acceptor-free film is $\sim 10^2$ times longer than the time window of our ultrafast transient absorption spectrometer, we attempted to measure carrier lifetimes using TCSPC for films with QD acceptor concentrations ranging from 0 to 6% but found no differences with increasing acceptors; in all cases, a subnanosecond decay dominates the TCSPC traces, and the longer time scale dynamics have no discernible trend with increasing acceptor concentration (Figure S8).[27] We conclude that rapid exciton dissociation and subsequent nonradiative recombination of carriers prevents a sufficient PLQY to obtain accurate carrier lifetimes. We instead used a continuous-wave (CW) laser

DOI: 10.1021/acs.nanolett.8b03020
Nano Lett. XXXX, XXX, XXX−XXX

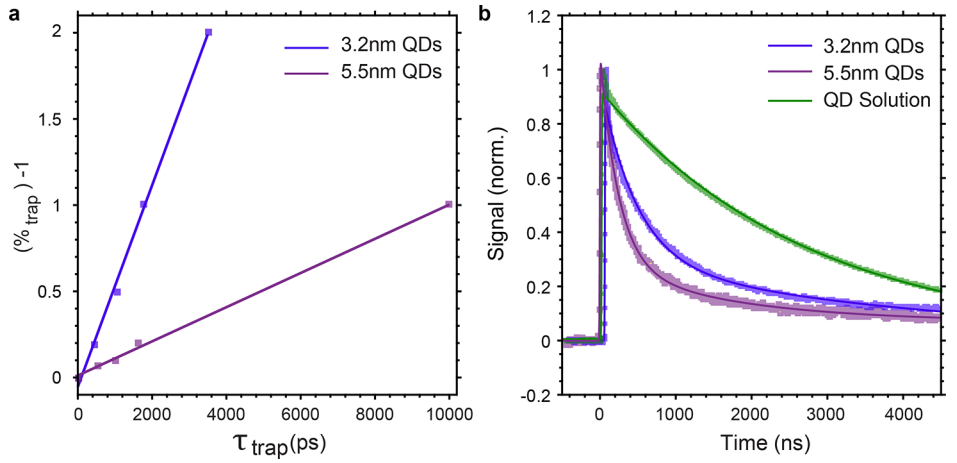

Figure 3. Mobilities and lifetimes for the two QD solids. (a) Linear fits of τ_{trap} versus N_t^{-1}, whose slope can be used to obtain diffusion coefficients and mobilities of the carriers. (b) Microsecond transients for pure donor QD films. Measurements on QDs in solution yield expected lifetimes of ~2−3 μs (Figure S9, Table S4).

Table 1. Transport Properties for the two QD solids

QD	τ (ns)	slope ($\%_{trap}^{-1}$ ps^{-1})	N_{traps} (cm^{-3})	D (cm^2 s^{-1})	μ (cm^2 V^{-1} s^{-1})	L_d (nm)	τ_{hop} (ps)
3.2 nm	437	5.8 (±0.6) × 10^{-4}	7.5 (±0.7)× 10^{14}	2.1 (±0.2)× 10^{-3}	8.0 (±0.8) × 10^{-2}	300 (±30)	8 ± 1
5.5 nm	240	9.9 (±0.7) × 10^{-5}	7.8 (±0.8) × 10^{15}	3.5 (±0.3) × 10^{-4}	1.4 (±0.1) × 10^{-2}	92 (±9)	48 ± 5

probe and directly recorded the transient absorption dynamics over a microsecond time range on a fast photodiode. Films are photoexcited by using the same ultrafast laser pulses as the mobility experiments and probed with a CW 980 or 1310 nm laser, depending on the bandgap of the donor QD. Transients require biexponential fits, where the first lifetimes range between 100−500 ns and correspond to the actual lifetime of the carriers, which is in good qualitative agreement with other reported lifetimes for PbS QD solids.[27,41] The second lifetimes are well over 1000 ns and are attributed to long-lived trapped carriers that can still contribute to the bleach signal (similar signals have been observed due to sub bandgap traps with μs lifetimes in lead halide perovskites).[45] Using ultrafast TA to measure diffusion coefficients and our modified TA setup to obtain carrier lifetimes, we can thus obtain the values needed for calculating diffusion lengths and interdot transfer rates.

Plots of N_t^{-1} versus τ_{trap} and transients measured over several microseconds are shown in Figure 3. Transport properties derived from these measurements are shown in Table 1 with bracketed values indicating uncertainty calculated from 95% confidence intervals (from the linear fits to the slope of τ_{trap} versus N_t^{-1}).

Key metrics can be extracted from the combination of the measured carrier lifetime (from the native acceptor-free film) and the τ_{trap} versus N_t^{-1} linear curves, including trap state density, the diffusion coefficient, and the carrier mobility. Trap state densities can be calculated by extrapolating the slope and using the measured carrier lifetimes to obtain the inverse trap percentage of the pure donor QD films, then multiplying the trap percentage by the bulk QD density 2 × 10^{19} cm^{-3} (calculated using an interdot spacing of 3.2 nm and a packing density of 64%).[25] The mobility of the 3.2 nm QDs are almost an order of magnitude higher than the larger 5.5 nm QDs. The smaller QDs also possess long carrier lifetimes of 437 ns, which in combination with a large diffusion coefficient yields a diffusion length of 300 ± 30 nm, which to our knowledge is the highest reported for PbS QD solids.[27] The same ligand exchange procedure and 3.2 nm QDs used in this study have been used to fabricate highly efficient QD solar cells with power conversion efficiencies up to 12.0%.[15] In contrast, the lower diffusion lengths and lifetimes obtained for the larger 5.5 nm QD films are consistent with the fact that when the same ligand exchange procedure was applied to larger QDs, the resulting photovoltaic devices exhibited a much lower performance of 3.5% PCE.[46] Considering both the shorter lifetimes and the lower mobilities of these films, we conclude that these active layers using larger QDs have higher trap state densities than films composed of smaller QDs.

To obtain interdot transfer times, the diffusion length can be related to τ_{hop} by the equation[24]

$$L_D = \sqrt{D\tau} = \sqrt{\frac{d^2}{6\tau_{hop}V_{th}\sigma N_t}} = d\sqrt{\frac{\tau_{trap}}{6\tau_{hop}}} \quad (9)$$

thus leading to τ_{hop} as

$$\tau_{hop} = \frac{\tau_{trap}}{6\left(\frac{L_D}{d}\right)^2} \quad (10)$$

These equations reflect an analytical treatment that is equivalent to the Miller-Abrahams hopping model,[47] which Gilmore et al. used in kinetic Monte Carlo simulations of PbS solids to obtain excellent fits of TA data in order to calculate interdot hopping rates.[28] Using the values obtained for lifetime and diffusion length, the interdot transfer times for the 3.2 and 5.5 nm QD films are 8 ± 1 and 48 ± 5 ps, respectively. Faster charge transfer for smaller sized QDs has been previously observed by Bozyigit et al. using temperature dependent current−voltage characterization of QD solids[48] and time-of-flight measurements supported by Monte Carlo simulations.[49]

A secondary confirmation of this ultrafast interdot transfer time derived from TA can be seen in the rate of spectral diffusion. Photoexcitation of the QD film creates a non-equilibrium distribution of excited carriers, owing to bandgap

DOI: 10.1021/acs.nanolett.8b03020
Nano Lett. XXXX, XXX, XXX−XXX

inhomogeneity resulting from QD polydispersity, as well as structural disorder within the QD matrix. Carriers on higher energy sites will rapidly migrate to lower energy sites to restore a Fermi−Dirac distribution. Gao et al. have reported such spectral diffusion within 2 ps for strongly coupled PbSe QD solids,[50,47] whereas Gilmore et al. measured spectral diffusion over 100s of ps in PbS QD solids that underwent solid-state ligand exchange with ethanethiol.[28] We have also previously reported spectral diffusion occurring in ∼300 ps for 3.2 nm PbS QD solids that were solution-exchanged with thioglycerol.[31]

We measure much more rapid spectral diffusion in our metal halide exchanged 3.2 nm PbS QD solids following photoexcitation at 930 nm, shown in Figure 4. To obtain a time constant for spectral diffusion, we use global analysis, whereby a sum of exponentials with associated time constants and wavelength dependent amplitudes are fitted to the TA map.[51] Here we obtain two decay associated spectra (DAS), shown in Figure 4b with their corresponding lifetimes. The shorter of the two time constants is 8 ps, and corresponds to the DAS with a shape that is antisymmetric around the bleach maximum, indicating transfer from higher to lower bandgap QDs. The second lifetime corresponds to an overall decay of the signal amplitude occurring on much longer time scales, attributable to carrier recombination within the film (although this time constant is poorly estimated owing to the limited time window for this experiment). Kinetic traces on either side of the center of the initial bleach peak are shown in Figure 4c. Signal at shorter wavelengths decays in parallel with rises at longer wavelengths as carriers move from higher to lower energy. Our spectral diffusion time constant of 8 ps is consistent with the time scale of the interdot hopping that was calculated from mobilities obtained using the acceptor QD quenchers. However, we note that spectral diffusion should always occur on faster time scales than the average interdot hopping since this process is strictly downhill. While there have been numerous reports of high carrier mobilities in large PbSe QD solids,[4,29,38,50,52] the rates of charge transfer found here are much higher than those previously found for PbS QD solids with short ligands,[42,50,53−55] which typically focus on QDs exchanged with mono- or bidentate thiol molecules. Our results show that using halide ligands instead of small molecules provides much higher mobility QD solids via solution-phase ligand exchanges.[14]

To further verify our measurements of interdot charge transfer rates, we performed ultrafast TA experiments on a 1:1 mixture of QDs with exciton resonances at 950 nm for the donor and 1060 nm for the acceptor, shown in Figure 5. For direct photoexcitation of the donor QDs at 950 nm, we observe a ∼20 ps (time constant obtained from global fitting) interdot transfer rate manifest as a rapid decay of the donor bandedge bleach and an identical but opposite increase in signal amplitude at the acceptor bandedge bleach. This matches well within the range of our calculated interdot hopping times, though may be longer potentially due to imperfect blending of the donor:acceptor QDs at such high acceptor concentrations (i.e., some electrons need more than one hop to reach an acceptor). When we instead directly photoexcite the acceptor QDs at 1100 nm, we observe a small amplitude population transfer with a time constant of ∼10 ps from acceptor to donor QDs. This supports our hypothesis that the valence band energies are similar for the various QD sizes used in this study, and thus we can observe a small transfer of population (holes) from larger to smaller dots, indicating that holes are not irreversibly trapped in the acceptor QDs. We carried out additional ultrafast TA experiments on films with larger acceptor QDs and donor/acceptor ratios of 1:2 and 1:4, and similarly find ultrafast decays of the donor exciton bleach signal (<10 ps), consistent with rapid charge transfer from donor to acceptor QDs in these films (Figure S10).

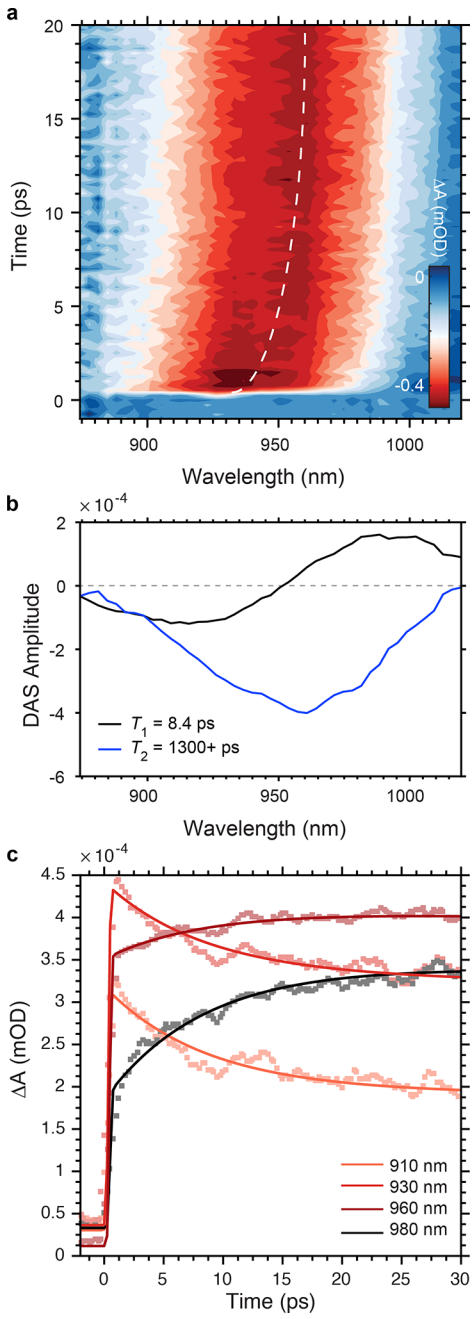

Figure 4. Ultrafast spectral diffusion in PbS QD solids. (a) TA map showing the red shifting of the bandedge bleach maximum with time (white line tracks the peak maximum). (b) Decay associated spectra and time constants obtained from global fitting. (c) Kinetic traces on either side of the bleach maximum. Fits were obtained using global analysis (Glotaran).[51] For clarity, raw data in these traces were smoothed using a moving average filter. Fits were obtained using the unsmoothed data.

DOI: 10.1021/acs.nanolett.8b03020
Nano Lett. XXXX, XXX, XXX−XXX

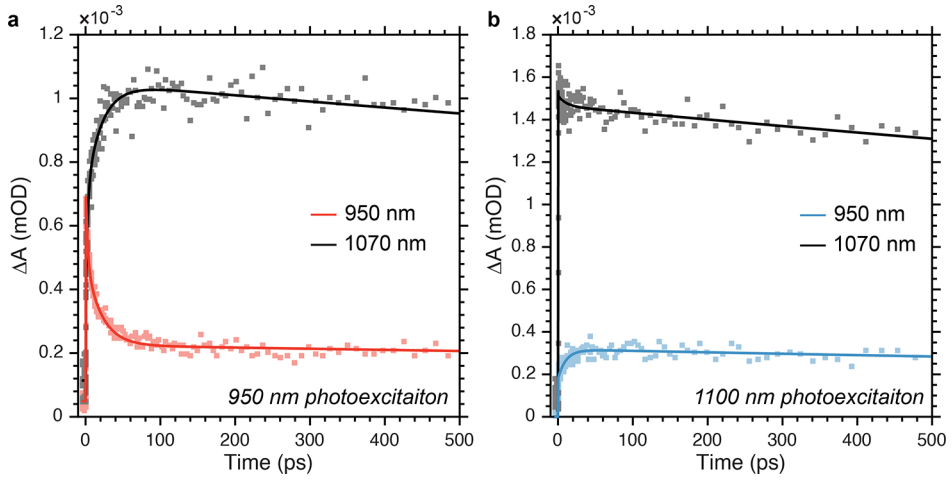

Figure 5. Ultrafast transient absorption of a 1:1 donor/acceptor blend. Probing the photoinduced carrier dynamics in a film composed of a 1:1 ratio of 950 nm (donor) and 1070 nm (acceptor) QDs. Although the difference in donor and acceptor bandgaps is not as large as used in the donor/acceptor experiments to determine mobility, here we are able to observe both donor and acceptor exciton resonances simultaneously in ultrafast TA experiments due to the shape of our white light probe spectrum. (a) Kinetic traces at the bandedge exciton bleaches for 950 nm bandgap (donor) and 1070 nm bandgap (acceptor) QDs following photoexcitation at 950 nm and (b) photoexcitation at 1100 nm (slightly red of the acceptor exciton maximum in order to avoid excitation of the donor QDs). Global fitting was used to obtain time constants of ∼20 ps for transfer from donor to acceptor dots, and ∼10 ps for transfer from acceptor to donor.

In summary, we have shown that TA can be used to overcome limitations of PL based methods to measure carrier mobilities, lifetimes, and diffusion lengths in low PLQY QD solids. We find diffusion lengths of ∼300 nm for solution exchanged QDs, which are the longest yet reported for PbS QD solids, and rapid interdot hopping times of ∼8 ps, among the fastest reported for these materials. These results help to correlate QD solar cell performance with carrier diffusion length and mobility and demonstrate the advantage of solution-based ligand exchanges over conventional solid-state layer-by-layer ligand exchange methods. We identify both lower mobilities and higher trap state densities in IR-bandgap 5.5 nm QD solids, which may account for their much lower power conversion efficiencies compared to NIR-bandgap 3.2 nm QD solids.

■ ASSOCIATED CONTENT

Supporting Information

The Supporting Information is available free of charge on the ACS Publications website at DOI: 10.1021/acs.nanolett.8b03020.

Methods for QD synthesis, ligand exchange, and film deposition; transient absorption measurements; atomic force microscopy; time-resolved photoluminescence (TCSPC); absorbance and photoluminescence spectra of colloidal quantum dots; AFM images; fluence dependence for TA experiments; trapping lifetimes for 5.5 nm QDs; time-resolved PL data; colloidal QD lifetimes from microsecond TA experiments; interdot transfer dynamics for a film of 1:1: mixture of donor/acceptor QDs (950 nm/1060 nm) (PDF)

■ AUTHOR INFORMATION

Corresponding Authors

*E-mail: ted.sargent@utoronto.ca.
*E-mail: o.voznyy@utoronto.ca.

ORCID

Andrew H. Proppe: 0000-0003-3860-9949
Randy P. Sabatini: 0000-0002-5975-4347
James Z. Fan: 0000-0002-1594-865X
Shana O. Kelley: 0000-0003-3360-5359
Oleksandr Voznyy: 0000-0002-8656-5074
Edward H. Sargent: 0000-0003-0396-6495

Notes

The authors declare no competing financial interest.

■ ACKNOWLEDGMENTS

This publication is based in part on work supported by the Ontario Research Fund Research Excellence Program, and by the Natural Sciences and Engineering Research Council (NSERC) of Canada (Discovery Grant 2016-06090). A.H.P. acknowledges support from the Fonds de recherche du Québec - Nature et technologies (FRQNT) and the Ontario Graduate Scholarship (OGS) program. The authors thank Mark W. B. Wilson and O. Ouellette for helpful discussions and L. Levina, E. Palmiano and D. Kopilovic for their help during the course of the study.

■ REFERENCES

(1) Liu, M.; Voznyy, O.; Sabatini, R.; García de Arquer, F. P.; Munir, R.; Balawi, A. H.; Lan, X.; Fan, F.; Walters, G.; Kirmani, A. R.; Hoogland, S.; Laquai, F.; Amassian, A.; Sargent, E. H. *Nat. Mater.* **2017**, *16*, 258.
(2) McDonald, S. A.; Konstantatos, G.; Zhang, S.; Cyr, P. W.; Klem, E. J. D.; Levina, L.; Sargent, E. H. *Nat. Mater.* **2005**, *4*, 138−142.
(3) Kamat, P. V. *J. Phys. Chem. C* **2008**, *112*, 18737−18753.
(4) Semonin, O. E.; Luther, J. M.; Choi, S.; Chen, H.-Y.; Gao, J.; Nozik, A. J.; Beard, M. C. *Science* **2011**, *334*, 1530.
(5) Chuang, C.-H. M.; Brown, P. R.; Bulović, V.; Bawendi, M. G. *Nat. Mater.* **2014**, *13*, 796−801.
(6) Lan, X.; Voznyy, O.; García de Arquer, F. P.; Liu, M.; Xu, J.; Proppe, A. H.; Walters, G.; Fan, F.; Tan, H.; Liu, M.; Yang, Z.; Hoogland, S.; Sargent, E. H. *Nano Lett.* **2016**, *16*, 4630−4634.
(7) Gong, X.; Yang, Z.; Walters, G.; Comin, R.; Ning, Z.; Beauregard, E.; Adinolfi, V.; Voznyy, O.; Sargent, E. H. *Nat. Photonics* **2016**, *10*, 253−257.

DOI: 10.1021/acs.nanolett.8b03020
Nano Lett. XXXX, XXX, XXX−XXX

(8) Shen, H.; Cao, W.; Shewmon, N. T.; Yang, C.; Li, L. S.; Xue, J. *Nano Lett.* **2015**, *15*, 1211−1216.
(9) Shirasaki, Y.; Supran, G. J.; Bawendi, M. G.; Bulovic, V. *Nat. Photonics* **2013**, *7*, 13−23.
(10) Konstantatos, G.; Howard, I.; Fischer, A.; Hoogland, S.; Clifford, J.; Klem, E.; Levina, L.; Sargent, E. H. *Nature* **2006**, *442*, 180−183.
(11) Hines, M. A.; Scholes, G. D. *Adv. Mater.* **2003**, *15*, 1844−1849.
(12) Clark, S. W.; Harbold, J. M.; Wise, F. W. *J. Phys. Chem. C* **2007**, *111*, 7302−7305.
(13) Ip, A. H.; Thon, S. M.; Hoogland, S.; Voznyy, O.; Zhitomirsky, D.; Debnath, R.; Levina, L.; Rollny, L. R.; Carey, G. H.; Fischer, A.; Kemp, K. W.; Kramer, I. J.; Ning, Z.; Labelle, A. J.; Chou, K. W.; Amassian, A.; Sargent, E. H. *Nat. Nanotechnol.* **2012**, *7*, 577−582.
(14) Yang, Z.; Janmohamed, A.; Lan, X.; García de Arquer, F. P.; Voznyy, O.; Yassitepe, E.; Kim, G.-H.; Ning, Z.; Gong, X.; Comin, R.; Sargent, E. H. *Nano Lett.* **2015**, *15*, 7539−7543.
(15) Xu, J.; Voznyy, O.; Liu, M.; Kirmani, A. R.; Walters, G.; Munir, R.; Abdelsamie, M.; Proppe, A. H.; Sarkar, A.; García de Arquer, F. P.; Wei, M.; Sun, B.; Liu, M.; Ouellette, O.; Quintero-Bermudez, R.; Li, J.; Fan, J.; Quan, L.; Todorovic, P.; Tan, H.; Hoogland, S.; Kelley, S. O.; Stefik, M.; Amassian, A.; Sargent, E. H. *Nat. Nanotechnol.* **2018**, *13*, 456.
(16) Williams, K. J.; Tisdale, W. A.; Leschkies, K. S.; Haugstad, G.; Norris, D. J.; Aydil, E. S.; Zhu, X. Y. *ACS Nano* **2009**, *3*, 1532−1538.
(17) Lan, X.; Masala, S.; Sargent, E. H. *Nat. Mater.* **2014**, *13*, 233−240.
(18) Choi, J.-H.; Fafarman, A. T.; Oh, S. J.; Ko, D.-K.; Kim, D. K.; Diroll, B. T.; Muramoto, S.; Gillen, J. G.; Murray, C. B.; Kagan, C. R. *Nano Lett.* **2012**, *12*, 2631−2638.
(19) Koh, W.-k.; Saudari, S. R.; Fafarman, A. T.; Kagan, C. R.; Murray, C. B. *Nano Lett.* **2011**, *11*, 4764−4767.
(20) Lhuillier, E.; Scarafagio, M.; Hease, P.; Nadal, B.; Aubin, H.; Xu, X. Z.; Lequeux, N.; Patriarche, G.; Ithurria, S.; Dubertret, B. *Nano Lett.* **2016**, *16*, 1282−1286.
(21) Zarghami, M. H.; Liu, Y.; Gibbs, M.; Gebremichael, E.; Webster, C.; Law, M. *ACS Nano* **2010**, *4*, 2475−2485.
(22) Liu, Y.; Gibbs, M.; Puthussery, J.; Gaik, S.; Ihly, R.; Hillhouse, H. W.; Law, M. *Nano Lett.* **2010**, *10*, 1960−1969.
(23) Hetsch, F.; Zhao, N.; Kershaw, S. V.; Rogach, A. L. *Mater. Today* **2013**, *16*, 312−325.
(24) Zhitomirsky, D.; Voznyy, O.; Levina, L.; Hoogland, S.; Kemp, K. W.; Ip, A. H.; Thon, S. M.; Sargent, E. H. *Nat. Commun.* **2014**, *5*, 3803.
(25) Zhitomirsky, D.; Voznyy, O.; Hoogland, S.; Sargent, E. H. *ACS Nano* **2013**, *7*, 5282−5290.
(26) Lee, E. M. Y.; Tisdale, W. A. *J. Phys. Chem. C* **2015**, *119*, 9005−9015.
(27) Carey, G. H.; Levina, L.; Comin, R.; Voznyy, O.; Sargent, E. H. *Adv. Mater.* **2015**, *27*, 3325−3330.
(28) Gilmore, R. H.; Lee, E. M. Y.; Weidman, M. C.; Willard, A. P.; Tisdale, W. A. *Nano Lett.* **2017**, *17*, 893−901.
(29) Talgorn, E.; Gao, Y.; Aerts, M.; Kunneman, L. T.; Schins, J. M.; Savenije, T. J.; van HuisMarijn, A.; van der ZantHerre, S. J.; Houtepen, A. J.; SiebbelesLaurens, D. A. *Nat. Nanotechnol.* **2011**, *6*, 733−739.
(30) Gao, J.; Zhang, J.; van de Lagemaat, J.; Johnson, J. C.; Beard, M. C. *ACS Nano* **2014**, *8*, 12814−12825.
(31) Yang, Z.; Fan, J. Z.; Proppe, A. H.; Arquer, F. P. G. d.; Rossouw, D.; Voznyy, O.; Lan, X.; Liu, M.; Walters, G.; Quintero-Bermudez, R.; Sun, B.; Hoogland, S.; Botton, G. A.; Kelley, S. O.; Sargent, E. H. *Nat. Commun.* **2017**, *8*, 1325.
(32) Du, H.; Chen, C.; Krishnan, R.; Krauss, T. D.; Harbold, J. M.; Wise, F. W.; Thomas, M. G.; Silcox, J. *Nano Lett.* **2002**, *2*, 1321−1324.
(33) McArthur, E. A.; Morris-Cohen, A. J.; Knowles, K. E.; Weiss, E. A. *J. Phys. Chem. B* **2010**, *114*, 14514−14520.
(34) Fan, J. Z.; Liu, M.; Voznyy, O.; Sun, B.; Levina, L.; Quintero-Bermudez, R.; Liu, M.; Ouellette, O.; García de Arquer, F. P.; Hoogland, S.; Sargent, E. H. *ACS Appl. Mater. Interfaces* **2017**, *9*, 37536−37541.
(35) Ouellette, O.; Hossain, N.; Sutherland, B. R.; Kiani, A.; García de Arquer, F. P.; Tan, H.; Chaker, M.; Hoogland, S.; Sargent, E. H. *ACS Energy Letters* **2016**, *1*, 852−857.
(36) Bi, Y.; et al. *Adv. Mater.* **2018**, *30*, 1704928.
(37) Liu, M.; Voznyy, O.; Sabatini, R.; Garcia de Arquer, F. P.; Munir, R.; Balawi, A. H.; Lan, X.; Fan, F.; Walters, G.; Kirmani, A. R.; Hoogland, S.; Laquai, F.; Amassian, A.; Sargent, E. H. *Nat. Mater.* **2017**, *16*, 258−263.
(38) Guyot-Sionnest, P. *J. Phys. Chem. Lett.* **2012**, *3*, 1169−1175.
(39) Liu, J.; Leng, J.; Wu, K.; Zhang, J.; Jin, S. *J. Am. Chem. Soc.* **2017**, *139*, 1432−1435.
(40) Proppe, A. H.; Quintero-Bermudez, R.; Tan, H.; Voznyy, O.; Kelley, S. O.; Sargent, E. H. *J. Am. Chem. Soc.* **2018**, *140*, 2890−2896.
(41) Hu, L.; Yang, Z.; Mandelis, A.; Melnikov, A.; Lan, X.; Walters, G.; Hoogland, S.; Sargent, E. H. *J. Phys. Chem. C* **2016**, *120*, 14416−14427.
(42) Choi, J. J.; Luria, J.; Hyun, B.-R.; Bartnik, A. C.; Sun, L.; Lim, Y.-F.; Marohn, J. A.; Wise, F. W.; Hanrath, T. *Nano Lett.* **2010**, *10*, 1805−1811.
(43) Miller, E. M.; Kroupa, D. M.; Zhang, J.; Schulz, P.; Marshall, A. R.; Kahn, A.; Lany, S.; Luther, J. M.; Beard, M. C.; Perkins, C. L.; van de Lagemaat, J. *ACS Nano* **2016**, *10*, 3302−3311.
(44) Klimov, V. I.; Mikhailovsky, A. A.; McBranch, D. W.; Leatherdale, C. A.; Bawendi, M. G. *Science* **2000**, *287*, 1011.
(45) Leijtens, T.; Eperon, G. E.; Barker, A. J.; Grancini, G.; Zhang, W.; Ball, J. M.; Kandada, A. R. S.; Snaith, H. J.; Petrozza, A. *Energy Environ. Sci.* **2016**, *9*, 3472−3481.
(46) Kiani, A.; Sutherland, B. R.; Kim, Y.; Ouellette, O.; Levina, L.; Walters, G.; Dinh, C.-T.; Liu, M.; Voznyy, O.; Lan, X.; Labelle, A. J.; Ip, A. H.; Proppe, A.; Ahmed, G. H.; Mohammed, O. F.; Hoogland, S.; Sargent, E. H. *Appl. Phys. Lett.* **2016**, *109*, 183105.
(47) Miller, A.; Abrahams, E. *Phys. Rev.* **1960**, *120*, 745−755.
(48) Bozyigit, D.; Lin, W. M. M.; Yazdani, N.; Yarema, O.; Wood, V. *Nat. Commun.* **2015**, *6*, 6180.
(49) Yazdani, N.; Bozyigit, D.; Yarema, O.; Yarema, M.; Wood, V. J. *J. Phys. Chem. Lett.* **2014**, *5*, 3522−3527.
(50) Gao, Y.; Talgorn, E.; Aerts, M.; Trinh, M. T.; Schins, J. M.; Houtepen, A. J.; Siebbeles, L. D. A. *Nano Lett.* **2011**, *11*, 5471−5476.
(51) Snellenburg, J. J.; Laptenok, S. P.; Seger, R.; Mullen, K. M.; van Stokkum, I. H. M. *J. Stat. Soft.* **2012**, *49*, 1−22.
(52) Talapin, D. V.; Murray, C. B. *Science* **2005**, *310*, 86.
(53) Borriello, C.; Miscioscia, R.; Mansour, S. A.; Di Luccio, T.; Bruno, A.; Loffredo, F.; Villani, F.; Minarini, C. *Phys. Status Solidi A* **2015**, *212*, 2677−2685.
(54) Klem, E. J. D.; Shukla, H.; Hinds, S.; MacNeil, D. D.; Levina, L.; Sargent, E. H. *Appl. Phys. Lett.* **2008**, *92*, 212105.
(55) Gilmore, R. H.; Winslow, S. W.; Lee, E. M. Y.; Ashner, M. N.; Yager, K. G.; Willard, A. P.; Tisdale, W. A. *ACS Nano* **2018**, *12*, 7741−7749.

DOI: 10.1021/acs.nanolett.8b03020
Nano Lett. XXXX, XXX, XXX−XXX